European Journal of Cell Biology xxx (xxxx) 151254

Contents lists available at ScienceDirect

European Journal of Cell Biology

journal homepage: www.elsevier.com/locate/ejcb

Extracellular vesicles from thyroid cancer harbor a functional machinery involved in extracellular matrix remodeling

Rocío del Carmen Bravo-Miana[a, b], María Florencia Soler[a, b], Danilo Guillermo Ceschin[c], Félix Royo[d], Dana María Negretti-Borga[a, b], Mikel Azkargorta[e], Félix Elortza[e], María del Mar Montesinos[a, b], Claudia Gabriela Pellizas[a, b], Juan Manuel Falcón-Pérez[d, f, 1, *], Ana Carolina Donadio[a, b, 1, **]

[a] Universidad Nacional de Córdoba, Facultad de Ciencias Químicas, Departamento de Bioquímica Clínica, Córdoba, Argentina
[b] Centro de Investigaciones en Bioquímica Clínica e Inmunología (CIBICI-CONICET), Ciudad Universitaria, Haya de la Torre y Medina Allende, Córdoba X5000HUA, Argentina
[c] Centro de Investigación en Medicina Traslacional Severo Amuchástegui, Instituto Universitario de Ciencias Biomédicas de Córdoba, Naciones Unidas 420, Parque Velez Sarsfield, Córdoba, Argentina
[d] Exosomes Laboratory, CIC bioGUNE-BRTA, CIBERehd, Bizkaia Technology Park, Derio 48160, Spain
[e] Proteomics Unit, CICbioGUNE-BRTA, CIBERehd, ProteoRed, Bizkaia Technology Park, Derio 48160, Bizkaia, Spain
[f] IKERBASQUE, Basque Foundation for Science, 48013 Bilbao, Spain

ARTICLE INFO

Keywords:
Extracellular vesicles
Thyroid cancer
Fibroblasts
Proteomics
MMP2
Co-cultures

ABSTRACT

Extracellular vesicles (EVs) participate in cell-stroma crosstalk within the tumor microenvironment and fibroblasts (Fb) contribute to tumor promotion in thyroid cancer. However, the role of tumor-stroma derived EVs still needs to be deciphered. We hypothesized that the interaction of thyroid tumor cells with Fb would liberate EVs with a specific proteomic profile, which would have an impact on EV-functionality in thyroid tumor progression-related events. Tumor (TPC-1, 8505c) and non-tumor (NThyOri) thyroid cells were co-cultured with human Fb. EVs, obtained by ultracentrifugation of conditioned media, were characterized by nanoparticle tracking analysis and western blotting. EV-proteomic analysis was performed by mass-spectrometry, and metalloproteinases (MMPs) were studied by zymography. EV-exchange was evaluated using immunofluorescence, confocal microscopy and FACS. EVs expressed classical exosome markers, with EVs from thyroid tumor cell-Fb co-cultures showing a proteomic profile related to extracellular matrix (ECM) remodeling. Bidirectional crosstalk between Fb and TPC-1 cells produced significantly more EVs than their isolated cells, and potentiated EV-functionality. In line with this, Fb-TPC-1 derived EVs induced MMP2 activation in NThyOri supernatants, and MMP2 activity could be evidenced in Fb and TPC-1 contact-independent co-cultures. Besides, MMP2 interactors allowed us to discriminate between EVs from thyroid tumoral and non-tumoral milieus. Interestingly, Fb internalized more EVs from TPC-1 than from NThyOri producing cells. Fb and thyroid tumor cell crosstalk produces specialized EVs with an ECM remodeling proteomic profile, enabling activation of MMP2 and possibly facilitating ECM-degradation, which is potentially linked with thyroid tumor progression.

Abbreviations: CAFs, cancer-activated fibroblasts; CI, contact-independent; CMs, conditioned media; DAPI, 4',6-diamidino-2-phenylindole; DEPs, differential enriched proteins; DEqMS, differential expression analysis of the quantitative mass spectrometry data; ECM, extracelular matrix; EVs, extracelular vesicles; FASP, filter-aided sample preparation; Fb, fibroblasts; FDR, false discovery rate; GO, gene ontology; MMPs, matrix metalloproteinases; nLC-MS/MS, nano-scale liquid chromatography coupled to tandem mass spectrometry; NTA, nanoparticle tracking analysis; ORA, over-representation analysis; PCoA, principal coordinate analysis; PPI, protein-protein interactions; PTC, papillary thyroid carcinoma; RT, room temperature; SFM, serum-free medium; TME, tumor microenvironment; TW, transwell; TW-CMs, transwell conditioned media

* Correspondence to: Exosomes Laboratory, CIC bioGUNE-BRTA, CIBERehd, Bizkaia Technology Park, Derio 48160, Spain.
** Correspondence to: Facultad de Ciencias Químicas, Universidad Nacional de Córdoba, Ciudad Universitaria, Haya de la Torre y Medina Allende s/n, Córdoba X5000HUA, Argentina.
E-mail addresses: jfalcon@cicbiogune.es (J.M. Falcón-Pérez), ana.carolina.donadio@unc.edu.ar (A.C. Donadio).
[1] Equal contribution.

https://doi.org/10.1016/j.ejcb.2022.151254
Received 16 March 2022; Received in revised form 29 June 2022; Accepted 30 June 2022
0171-9335/

1. Introduction

From the first stages of tumor initiation, malignant cells interact with resident and recruited host cells and the extracellular matrix (ECM), as well as with soluble factors in the tumor microenvironment (TME). These multiple interactions, which reprogram the phenotype of both interactive partners, include cell-to-cell contact, growth factor and cytokine signaling, and extracellular vesicles (EVs) exchanging bioactive molecules (Maman and Witz, 2018).

EVs constitute heterogeneous populations of nano-sized vesicles typically classified according to their cellular biogenesis (van Niel et al., 2018) or just based on their size, defined as small- (50–200 nm) or large-EVs (200 nm-2 μm) (Kowal et al., 2016). In 2019, Jeppesen and coworkers (Jeppesen et al., 2019) introduced a sub-classification of classical and non-classical exosomes into the small-EVs, based on the presence of the exosomal markers CD63, CD81, and CD9. Before their release, EVs are packed with bioactive molecules, including proteins, lipids, and nucleic acids. Importantly, interactions of EVs with recipient cells may regulate their pathophysiological state.

In tumors, ECM remodeling, including ECM deposition, crosslinking and degradation, creates a cancer permissive microenvironment, increasing the bioavailability of ECM-bound biomolecules. Among the main drivers of ECM degradation are the matrix metalloproteinases (MMPs), produced by both stromal and tumor cells (Winkler et al., 2020). Considering the tumor stroma cells, fibroblasts (Fb) produce and degrade ECM (Sahai et al., 2020), and they are also key elements that play a role in cell-to-cell communication. Interestingly, Bertero and coworkers (Bertero et al., 2019) described that the metabolic crosstalk between tumor-associated Fb and cancer cells sustains cancer cell proliferation, while promoting ECM remodeling activity from Fb.

Thyroid cancer is the most prevalent malignant disease of the endocrine system and originates principally from follicular cells. Papillary thyroid carcinoma (PTC), a differentiated thyroid cancer, is the most frequent type, sometimes slow-growing but with local lymph node compromise. The anaplastic thyroid carcinoma, a dedifferentiated thyroid cancer, presents a fast growth and the highest aggressiveness, with a poor prognosis and resistance to cancer treatments (Fozzatti and Cheng, 2020). The incidence of thyroid cancer has increased gradually but continuously since the 1980s, though apparently becoming stabilized from 2015 onwards (Siegel et al., 2021). Nevertheless, there is an increasing tendency for larger and more advanced PTCs to be detected, accompanied by a significant increase in thyroid cancer mortality (Kitahara and Sosa, 2020).

In thyroid cancer, the role of TME in tumor development is beginning to be clarified. In this sense, using experimental models, Fb recruitment and ECM remodeling in the tumor milieu have been emphasized as being key features for thyroid tumor progression (Jolly et al., 2016; Saitoh et al., 2009). In agreement, Minna and coworkers (Minna et al., 2020) described an enriched expression of αSMA in human PTC tissues, as being indicative of cancer-activated fibroblasts (CAFs). Similarly, our laboratory reported that soluble factors present in the conditioned media (CMs) of CAFs promoted the proliferation and invasion of the follicular thyroid cancer cell line FTC-133 (Fozzatti et al., 2019). More recently, by using an in vitro co-culture model, we described that Fb-thyroid tumor cell interaction promotes thyroid tumor cell migratory phenotype and MMP2 and MMP9 expression in CMs (Bravo-Miana et al., 2020). This study also demonstrated the presence of EVs from thyroid tumor cell-Fb interacting cells and their capacity to modify the proteolytic performance of normal recipient Fb, revealing distinctive characteristics between EVs secreted from tumoral and those from non-tumoral thyroid milieu.

Considering these results, in the present work, we aimed to characterize the EVs produced by Fb, as well as by isolated- and Fb-co-cultured tumoral and non-tumoral thyroid cells, to study the role of tumor-Fb crosstalk in the EV protein cargo and biological function.

2. Material and methods

2.1. Cell lines, Fb-thyroid cell contact-dependent co-cultures and EVs isolation

The human papillary thyroid cancer cell line (TPC-1) was purchased from the University of Colorado Cancer Center Cell Bank. The human anaplastic thyroid cancer cell line (8505c) and the non-tumor thyroid cell line (NThyOri) were kindly donated by Dr. Pilar Santisteban (Instituto de Investigaciones Biomédicas Alberto Sols, Madrid, Spain) and authenticated by STR genotyping using PowerPlex Fusion System (Promega) at the Centro de Excelencia en Procesos y Productos de Córdoba (Córdoba, Argentina). In accordance with Bravo-Miana and coworkers (Bravo-Miana et al., 2020), normal human Fb were obtained from skin biopsies from anonymized healthy volunteers, with the protocol being approved by the Ethical Committee of Hospital Nacional de Clínicas, Universidad Nacional de Córdoba, and used as stromal representative cells. Cells were also regularly tested for mycoplasma contamination using in-house PCR assays. Fb, TPC-1, 8505c were maintained in DMEM medium (Gibco, Life Technologies) and NThyOri in RPMI medium 1640 (Gibco, Life Technologies) both supplemented with 10% v/v fetal bovine serum (FBS, Gibco, Life Technologies) and 100 units/mL penicillin-0.1 mg/mL streptomycin (Gibco, Life Technologies), at 37 °C and 5% of CO_2. TPC-1, 8505c and NThyOri (600,000 cells) were co-plated with Fb (600,000 cells) in 100-mm-diameter plates; and the expressions 'Fb-TPC-1', Fb-8505c' and 'Fb-NThyOri' are used to indicate the contact-dependent co-cultures between Fb and their corresponding thyroid cells. Isolated Fb, TPC-1, 8505c, and NThyOri (600,000 cells) cells were seeded as controls of their corresponding co-cultures. First, the cells were cultured in a serum-supplemented medium for 72 h. Then, cell-monolayers were washed two times with warm Dulbecco's modified phosphate-buffered saline (PBS) to finally, being incubated with serum-free medium (SFM, 9 mL/plate) for 48 h. The CMs were collected, cooled to 4 °C, and processed to obtain the EVs as previously described (Bravo-Miana et al., 2020). The pellets of EVs were resuspended in 60–100 μL of PBS and stored at − 80 °C for further analysis. For functional studies, the EVs were maintained at 4 °C and used immediately after being obtained. Fig. S1, shows the experimental workflow.

2.2. Nanoparticle tracking analysis and western blotting

The size and concentration of the EVs were determined by nanoparticle tracking analysis (NTA), using a NanoSight LM10 system (Royo et al., 2017). Biochemical characterization of the EVs (5 μg of EVs lysates, quantified using Bradford assay) was performed by western-blotting analysis under non-reducing conditions, as previously described (Royo et al., 2017). Primary mouse monoclonal antibodies against CD63 (clone H5C6, #556019, RRID:AB_396297; 1/1000), FLOT-1 (#610820, RRID:AB_398139; 1/1000), GRP78 (#610979, RRID:AB_398292; 1/250), and GM130 (#610822, RRID:AB_398142; 1/250) were purchased from BD Biosciences, CD9 (MAB1880, RRID:AB_2075900; 1/1000) from R&D Systems, and β-actin from Santa Cruz Biotechnology (sc-69879, RRID:AB_1119529; 1/1000). The secondary anti-mouse HRP-conjugated antibody (#315-035-045, RRID:AB_2340066; 1/6000) was purchased from Jackson ImmunoResearch.

2.3. Proteomic analysis

EV samples were incubated in a buffer containing 7 M urea, 2 M Thiourea, 4% CHAPS and 5 mM DTT. Proteins (200 ng) were digested in solution following a filter-aided sample preparation (FASP) protocol (Wisniewski et al., 2009), with minor modifications. Briefly, trypsin was added at a trypsin:protein ratio of 1:50, and the mixture was incubated overnight at 37 °C, dried out in a RVC2 25 speedvac concentrator,

and resuspended in 0.1% formic acid. Peptides were further desalted and resuspended in 0.1% formic acid using C18 stage tips (Millipore). Samples were analyzed in a novel and high-resolution hybrid trapped ion mobility spectrometry–quadrupole time of flight mass spectrometer (timsTOF Pro with PASEF, Bruker Daltonics), coupled online to a nanoElute liquid chromatograph (Bruker). The EV samples (200 ng) were directly loaded in a 15 cm Bruker nanoelute FIFTEEN C18 analytical column (Bruker) and resolved at 400 nl/min with a 30 min gradient (0–35% acetonitrile, where mobile phase A was water containing 0.1% v/v formic acid, while mobile phase B was acetonitrile containing 0.1% v/v formic acid).

Protein identification and quantification were carried out using PEAKS software (Bioinformatics solutions). Searches were carried out using a database consisting of human entries (Uniprot/Swissprot 2020_04, 20375 entries), with precursor and fragment tolerances of 20 ppm and 0.05 Da. Trypsin was considered as the digestion enzyme, and two missed cleavages were allowed. Oxidation of methionines was considered as a variable modification, and carbamidomethylation of cysteines as a fixed modification. A search against the decoy database was conducted in order to estimate the false discovery rate (FDR), with only peptides identified with FDR < 1% being kept. For the quantitative analysis, only proteins identified with at least two peptides with FDR < 1% were considered in the study. Data was loaded onto the Perseus platform (https://maxquant.net/perseus/, RRID:SCR_015753) (Tyanova et al., 2016) and further processed: log2 transformed, filtered for reproducibility (two out of three intensity-valid values, identified in biological triplicates, in at least one group of samples), and imputated.

2.4. Statistical and bioinformatic proteome analysis

The bioinformatic analysis used the human Vesiclepedia database (http://microvesicles.org/, 2020_10, RRID:SCR_019011) (Pathan et al., 2019) to make comparisons between annotated data and the experimental EV-proteome. FASTA files of all the identified proteins were uploaded to Signal P 4.1 servers (RRID:SCR_015644) to predict the presence of signal peptide cleavage sites (Petersen et al., 2011). Next, an analysis using the Gene Ontology (GO) database against cellular components of all identified proteins was performed, utilizing FunRich Software (http://www.funrich.org/, RRID:SCR_014467) (Pathan et al., 2017). Data were exported to R software v3.3.2 (http://cran.r-project.org, RRID:SCR_001905) to conduct statistical and principal coordinate analysis (PCoA), to generate a heatmap and matrix correlations, and to apply the DEqMS (differential expression analysis of the quantitative mass spectrometry data) method (Zhu et al., 2020), using the ggplot2 (RRID:SCR_014601) and Bioconductor (RRID:SCR_006442) packages. DEqMS pipeline analysis with Benjamini-Hochberg multiple testing FDR correction allowed the differential enriched proteins (DEPs) in the EV-proteome to be obtained, using the following established comparisons:

(1) TPC-1 and 8505c vs. NThyOri cells, and vice versa,
(2) Fb-TPC-1 and Fb-8505c co-cultures vs. Fb-NThyOri co-culture and vice versa, and
(3) Fb-TPC-1, Fb-8505c, and Fb-NThyOri co-cultures vs. their isolated thyroid cells.

Adj. p-values < 0.001 and FC ≥ 2 for comparisons (1) and (2), and adj. p < 0.01 and FC ≥ 2 for comparison (3) were considered statistically significant. The lists of DEPs (Tables S1-S5) and over-representation analysis (ORA) were used to detect statistically significantly enriched terms, using g:profiler webtool (https://biit.cs.ut.ee/gprofiler/gost, RRID:SCR_006809), related with GO (biological process and molecular function terms) and Reactome databases. Datasets returned by g:Profiler were visualized and interpreted using the EnrichmentMap plug-in v3.3.1 (RRID:SCR_016052), ClusterMaker2 and AutoAnnotate v1.3.3 run on Cytoscape v3.8.2 (RRID:SCR_003032) (Reimand et al., 2019). Finally, published or predicted protein-protein interactions (PPI) were searched, using the String database (RRID:SCR_005223) in Cytoscape (Szklarczyk et al., 2019), between EV-proteins that presented a significant PPI score with a high confidence score cut off > 0.7 and MMP2 (MMP2 interactors).

2.5. NThyOri EV-stimulation assay

NThyOri (150,000 cells) were seeded in six-well culture plates until confluence. The NThyOri monolayers were then washed with PBS and stimulated for 24 h with the pelleted EVs obtained from the same number of EV-secreting Fb, TPC-1, NThyOri and Fb-TPC-1 or Fb-NThyOri cells (Tkach et al., 2018). Those EV pellets were resuspended in 2.0 mL of SFM, and as control, SFM was added to another set of NThyOri cells. After 24 h of incubation, the CMs were collected, cleared of intact cells and cell debris (10,000x g), and saved at − 80 °C for zymography.

2.6. Fb and TPC-1 EV-uptake assay

For the EV-uptake assay, EV-secreting cells were stained with 1 mM Vybrant™ DiI or DiO Cell-Labelling Solution (V-22885, V-22886, Invitrogen). Briefly, Fb, TPC-1, 8505c and NThyOri cell-monolayers (in 100-mm-diameter plates in SFM, at 80% confluence) were incubated with 5 μL DiI/mL (Fb) or 5 μL DiO/mL (TPC-1, 8505c and NThyOri cells) for 4 h at 37 °C. After incubation, the culture media were discarded, cell monolayers were washed with PBS to remove the excess dye, and the cells were collected for the assay. Fb (100,000 cells) or TPC-1 (40,000 cells) recipient cells were seeded in the lower chamber of a six-transwell (TW) system (0.4 μm pore size; Corning-Costar). Isolated Fb^{DiI}, $TPC\text{-}1^{DiO}$, $8505c^{DiO}$, $NThyOri^{DiO}$ (40,000 cells) and their corresponding Fb^{DiI}-$TPC\text{-}1^{DiO}$, Fb^{DiI}-$8505c^{DiO}$, Fb^{DiI}-$NThyOri^{DiO}$ (40,000 cells + 40,000 cells) co-cultures were transferred to the upper chambers of the TW. Alternatively, Fb or TPC-1 recipient cells were grown on 11 mm-uncoated glass coverslips in the lower chambers of the TW system. Contact-independent (CI) co-cultures were incubated for 72 h in a serum supplemented medium, followed by 48 h of incubation in SFM. The EV-uptake by recipient cells was evaluated using indirect immunofluorescence, confocal microscopy, and flow cytometry. Lower chamber transwell CMs (TW-CMs) were harvested for zymography. As controls, Fb or TPC-1 recipient cells were cultured with unlabeled cells in the upper chamber (negative controls). For positive controls, 1 μL of DiI or DiO/mL of HG-DMEM was added to the cell-free upper chambers.

2.7. Immunofluorescence and confocal microscopy

After culture, recipient cells grown on 11 mm-uncoated coverslips were washed with PBS and fixed in 2% formaldehyde for 20 min at room temperature (RT). Coverslips were then washed, incubated with 0.7 μg/mL 4',6-diamidino-2-phenylindole (DAPI), and finally mounted with 10 μL Fluormount-G (0100-01, Southern Biotech). Images were acquired on an Axio imager D1 (ZEISS, Oberkochen, Germany). Alternatively, for studying the intracytoplasmic localization of the EVs, fixed coverslips were immunostained with mouse monoclonal antibody against CD81 (clone Js-81, #555675, RRID:AB_396028, 1/500; BD Biosciences) overnight at 4 °C and washed three times with PBS. As secondary antibodies, anti-mouse Cy™3-conjugated (#715-165-150, RRID:AB_2340813, 1/500; Jackson ImmunoResearch) or Alexa Fluor® 488 (A-21202, RRID:AB_141607, 1/500; Invitrogen) was used. Finally, the coverslips were washed and mounted, with images being acquired using an Fv1200 confocal microscope (Olympus Life Sciences) with x60 and x100 oil immersion objectives. All images were processed using FIJI-ImageJ software (RRID:SCR_002285; National Institutes of Health, Bethesda, MD).

2.8. EV-uptake quantification by flow cytometry

After culture, Fb and TPC-1 recipient cells, grown in the lower chambers of the TW system, were washed with PBS and detached with 0.3 mL (Fb) or 0.6 mL (TPC-1) of 1X TrypLE Select (12563011, Gibco). Flow cytometry was performed with a BD FACSCanto II instrument (BD Biosciences, San Jose, USA), and 10000 (Fb) and 50000 (TPC-1) events were acquired using a 5000 threshold. The DiI dye (red) was read on the PE channel (578 nm), and DiO (green) on the FITC channel (520 nm). Data analysis was performed using FlowJo X software (RRID:SCR_008520) and comparisons were made among the data obtained with the same fluorophore.

2.9. Zymography

Gelatinolytic activity in the CMs (40 μL) from NThyOri EV-stimulated cells was analyzed by zymography, as previously described (Bravo-Miana et al., 2020). On the other hand, TW-CMs (8 μL) were evaluated using a pre-cast zymogram assay (15605608, Novex Zymogram Gels, Life Technologies), following the manufacturer's instructions. Areas of protease activity appear as clear bands against a dark background.

2.10. Statistical analysis

Results were expressed as mean ± SEM from at least three independent experiments. The statistical significance of differences among means was determined by a parametric or non-parametric ANOVA test, and by an unpaired t-test using Graph-Pad Prism 6.0 (RRID:SCR_002798; GraphPad Software). Differences were considered statistically significant at $p < 0.05$.

3. Results

3.1. Characterization of EVs from isolated Fb, thyroid cell and Fb-thyroid cell co-cultures

EVs from Fb, TPC-1, 8505c, and NThyOri isolated cells, as well as from Fb-TPC-1, Fb-8505c, and Fb-NThyOri co-cultures, were quantified and morphometrically and biochemically characterized. Regarding size determination (NTA), most of the EVs obtained from isolated or co-cultured cells presented a size that ranged from 50 to 200 nm. No significant size differences could be detected among EVs from co-cultured or isolated cells (Fig. 1A, B). In agreement, previous results using transmission electronic microscopy showed the characteristic cup-shaped morphology of EVs from isolated and co-cultured cells, with the 80–90% of the vesicles of the size described for small-EVs (i.e. 50–200 nm) (Bravo-Miana et al., 2020).

In addition, among isolated cells, 8505c produced a significantly higher quantity of EVs/10^6-secreting cells than TPC-1 or Fb ($1.4 \times 10^9 \pm 3.5 \times 10^8$ vs $2.7 \times 10^8 \pm 5.7 \times 10^7$ and vs $2.9 \times 10^8 \pm 7.6 \times 10^7$; $p < 0.05$, respectively; Fig. 1C). With respect to the number of EVs produced by Fb-thyroid cell co-cultures, no significant differences were registered among Fb-TPC-1, Fb-8505c, and Fb-NThyOri. Regarding the EVs released by co-cultured cells in relation with their corresponding isolated cultured cells, Fb-TPC-1 delivered a significantly higher number of EVs/10^6 cells than isolated TPC-1 and Fb ($8.5 \times 10^8 \pm 1.7 \times 10^7$ vs. $2.7 \times 10^8 \pm 5.7 \times 10^7$ and vs $2.9 \times 10^8 \pm 7.6 \times 10^7$; $p < 0.01$ and $p < 0.05$, respectively). In contrast, although Fb-8505c produced a significantly higher number of EVs in comparison with Fb, no significant differences were found when compared to the number of EVs released by 8505c cells. Finally, no differences were detected among Fb-NThyOri and Fb or NThyOri isolated cells. EVs revealed the expression of the classical exosome markers CD63, CD9, and FLOT-1, with these proteins being enriched in EVs with respect to cell lysates; in addition to the previously described expression of CD81 (Bravo-Miana et al., 2020). Interestingly, CD63 appeared highly enriched in EVs from Fb-TPC-1 and Fb-8505c compared to EVs from Fb-NThyOri. GRP78 and GM130, which revealed a lack of cellular debris contamination, were not detected in the EV preparations (Fig. 1D and Suppl. Fig. S2).

3.2. Comparative proteomic analysis of EVs from isolated Fb, thyroid cell and Fb-thyroid cell co-cultures

To compare the EV-protein cargo among isolated Fb, TPC-1, 8505c, NThyOri, and Fb-TPC-1, Fb-8505c and Fb-NThyOri co-cultured cells, the EVs (biological triplicates) were analyzed by nano-scale liquid chromatography couped to tandem mass spectrometry (nLC-MS/MS). The results obtained identified 1977 proteins; 98% of the EV-protein cargo has been previously reported in EVs, and 97 out of the 100-most frequent proteins previously annotated in the Vesiclepedia database were identified, thereby confirming EV-enrichment in the EV samples (Fig. 2A). GO analysis of cellular components revealed a significant enrichment of the identified EV-proteins related to EVs (45.5%), membrane (32.7%), cytosol (53.7%) among other cellular components, and also supported EV-isolation (Fig. 2B). Subsequent analysis using Signal P 4.1 software showed that 1533 out of 1977 proteins did not present the predicted signal peptide in their polypeptidic sequences.

A PCoA, using the top 100 identified EV-proteins, demonstrated the similarity of biological triplicates with no outlier samples within each cluster, and showed segregation between TPC-1/Fb-TPC-1, 8505c/Fb-8505c and NThyOri/Fb-NThyOri (Fig. 2C). Unsupervised hierarchical clustering, based on the average intensity of the top 100 identified EV-proteins, revealed the segregation between Fb-EVs with isolated and co-cultured thyroid cells, and confirmed clustering among EV samples from biological triplicates. More interestingly, a segregation between TPC-1/Fb-TPC-1 regarding the 8505c/Fb-8505c and NThyOri/Fb-NThyOri EV samples was evidenced (Fig. 2D). These findings were reinforced by the Pearson correlation analysis, as displayed in Fig. 2E using the 1977 identified proteins. As stated above, segregation of the proteomic EV-datasets into three main clusters was shown, two based on the EV-proteome from thyroid cells and their co-cultures, and another comprising the EV-proteome of Fb. Furthermore, the analysis of the correlation indexes revealed a close association between the proteomic datasets of EVs from Fb-8505c and Fb-NThyOri with their corresponding thyroid isolated cell EV-proteomic dataset ($r = 0.96$ and 0.93–0.95, respectively). However, although a strong correlation between the EV-proteomic datasets of Fb-TPC-1 vs. TPC-1 was also detected, the r indexes ($r = 0.85$–0.91) suggest that Fb co-culturing provides an additional source of variability.

3.3. EVs from Fb-thyroid tumor cell co-culture participate mainly in extracellular matrix remodeling

In all, 97 DEPs in EVs from TPC-1 vs EVs from NThyOri (Table 1 and Table S1A) were detected. The ORA revealed significant enrichments in several clusters of terms in TPC-1-derived DEPs, such as MET and PTK2 signaling, heparan sulfate metabolism, ECM organization and interactions, and platelet degranulation, among others (Fig. 3A). In turn, 61 DEPs were detected in Fb-TPC-1 vs. Fb-NThyOri-derived EVs (Table 1 and Table S2A), and interestingly, these showed a significantly enriched convergence in one cluster, related to ECM organization, degradation and interaction terms (Fig. 3B). The same strategy was used to compare the DEPs between EVs derived from: (1) NThyOri vs. TPC-1 isolated cells and (2) Fb-NThyOri vs Fb-TPC-1 co-cultured cells (Table 1; Table S1B and S2B). This analysis showed that the clusters of terms obtained in both comparisons were similarly related to the maintenance of cellular metabolism (data not shown). The ORA analyses of DEPs between EVs derived from 8505c vs. NThyOri isolated cells revealed 48 DEPs (Table 1 and Table S3A) that converged on five clusters

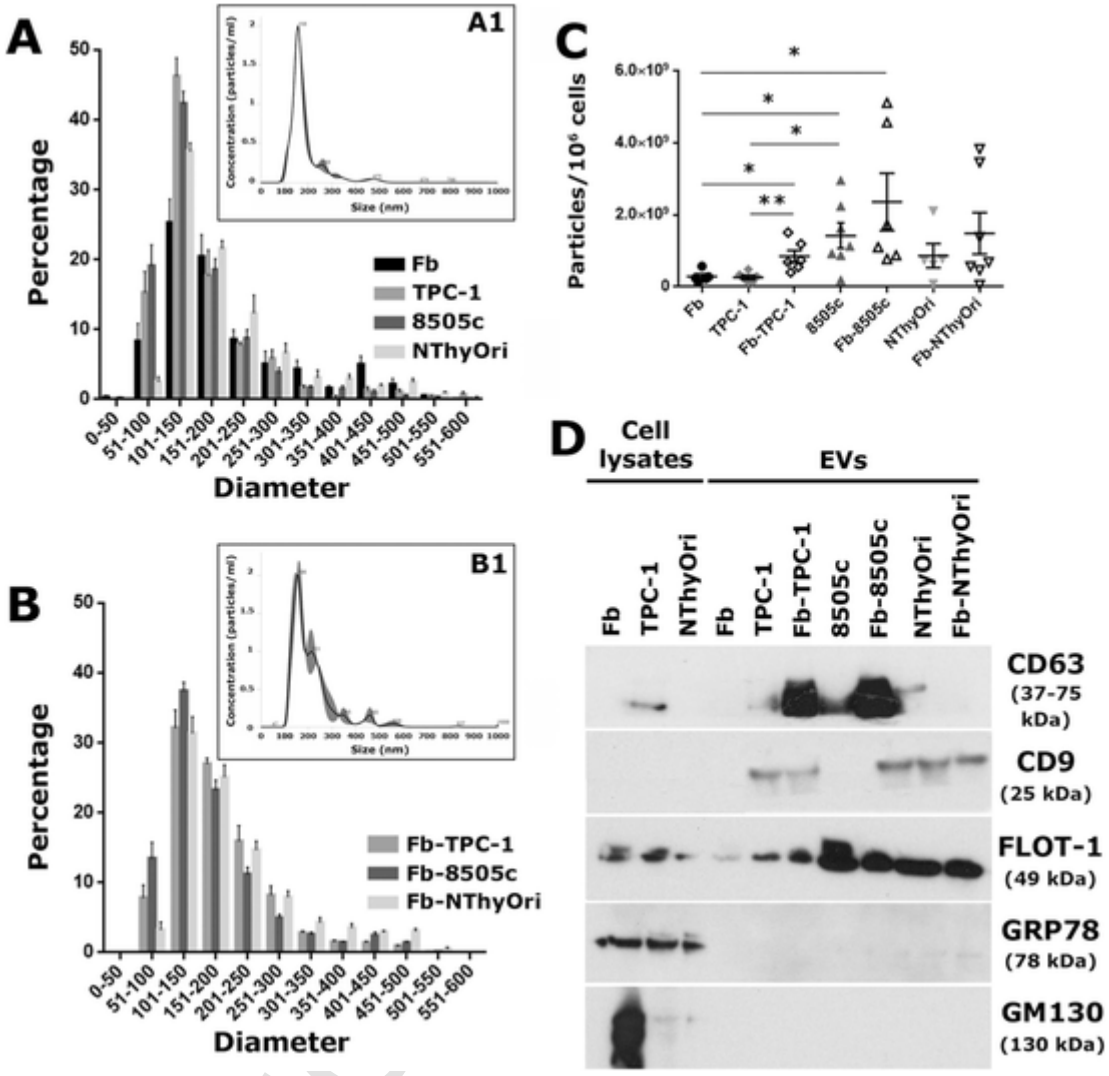

Fig. 1. Morphometric, quantitative and biochemical characterization of EVs from Fb, thyroid cells and Fb-thyroid cell co-cultures. Size distribution of EVs from (A) isolated Fb, TPC-1, 8505c and NThyOri cells and (B) Fb-TPC-1, Fb-8505c and Fb-NThyOri co-cultures. Insets show the representative size profile determined by NTA from (A1) TPC-1 and (B1) Fb-TPC-1. (C) Quantification by NTA of the number of particles per 10^6 EV-secreting cells released from Fb, TPC-1, 8505c and NThyOri isolated cells, and from Fb-TPC-1, Fb-8505c and Fb-NThyOri co-cultured cells. A significantly higher quantity of EVs from 8505c vs TPC-1 and Fb (* $p < 0.05$; Kruskal-Wallis test, Dunn's post test), from Fb-TPC-1 vs TPC-1 and Fb (**$p < 0.01$; * $p < 0.05$ respectively, Kruskal-Wallis test, Dunn's post test) and from Fb-8505c vs Fb (* $p < 0.05$, Kruskal-Wallis test, Dunn's post test) were observed. Data are presented as the mean value of at least five independent experiments (mean ± SEM). (D) Western blotting assay of EV (CD63, CD9, FLOT-1) and non-EV (GRP78 and GM130) proteins in EVs and cell lysates.

of terms related with ECM organization and ECM binding, among others. (Fig. 3C). When Fb-8505c- and Fb-NThyOri-derived EVs were compared, ECM organization, degradation and interactions were evidenced (Table 1 and Table S4A; Fig. 3D). Finally, DEPs obtained on comparing NThyOri vs. 8505c (Table 1 and Table S3B) and Fb-NThyOri vs. Fb-8505c (Table 1 and Table S4B) did not show enriched terms to note. Among the DEPs in EVs from both Fb-TPC-1 and Fb-8505c, CD63 was one of the over-represented proteins, in agreement with western blot results.

3.4. Fb and TPC-1 crosstalk releases specialized EVs that induce MMP2 activation in NThyOri cells

Previously reported results have described that only EVs derived from thyroid tumor cell-Fb interacting cells modified the proteolytic performance of normal recipient Fb (Bravo-Miana et al., 2020). These findings prompted us to identify and compare DEPs and their potential functionality in EVs derived from tumor Fb-TPC-1, Fb-8505c and Fb-NThyOri co-cultures with EVs from isolated thyroid cells (TPC-1, 8505c, and NThyOri, respectively). The DEPs (Table 1 and Table S5), among the three data sets, are presented using a Venn diagram. Further examination showed 25 DEPs in the Fb-TPC-1 vs. TPC-1 set, with only 5 in the Fb-8505c vs. 8505c set, and 23 DEPs in the Fb-NThyOri vs. NThyOri set (Fig. 4A). The ORA analysis carried out with DEPs from the Fb-TPC-1 vs. TPC-1 set showed that proteins were focally associated with ECM and collagen degradation (Fig. 4A1).

Among MMPs, MMP2 has been associated with ECM remodeling, collagen IV degradation and tumor angiogenesis during cancer progression (Quintero-Fabian et al., 2019). Moreover, MMP2 has been pointed as a predictive marker for PTC (Shi et al., 2018). Regarding this, we evaluated the ability of EVs from Fb-TPC-1 as well as from Fb, TPC-1, NThyOri and Fb-NThyOri co-cultured cells, to induce MMP2 secretion and activation in NThyOri cells (Fig. 4B). In agreement with previous findings (Bravo-Miana et al., 2020), a remarkable increase in active MMP2 in NThyOri CMs was registered upon stimulation with EVs from Fb-TPC-1 compared with EVs from TPC-1 cells (Fig. 4C and D). Interestingly, no changes in proMMP2 or MMP2 activity were detected when NThyOri were incubated with EVs from isolated Fb, NThyOri or Fb-

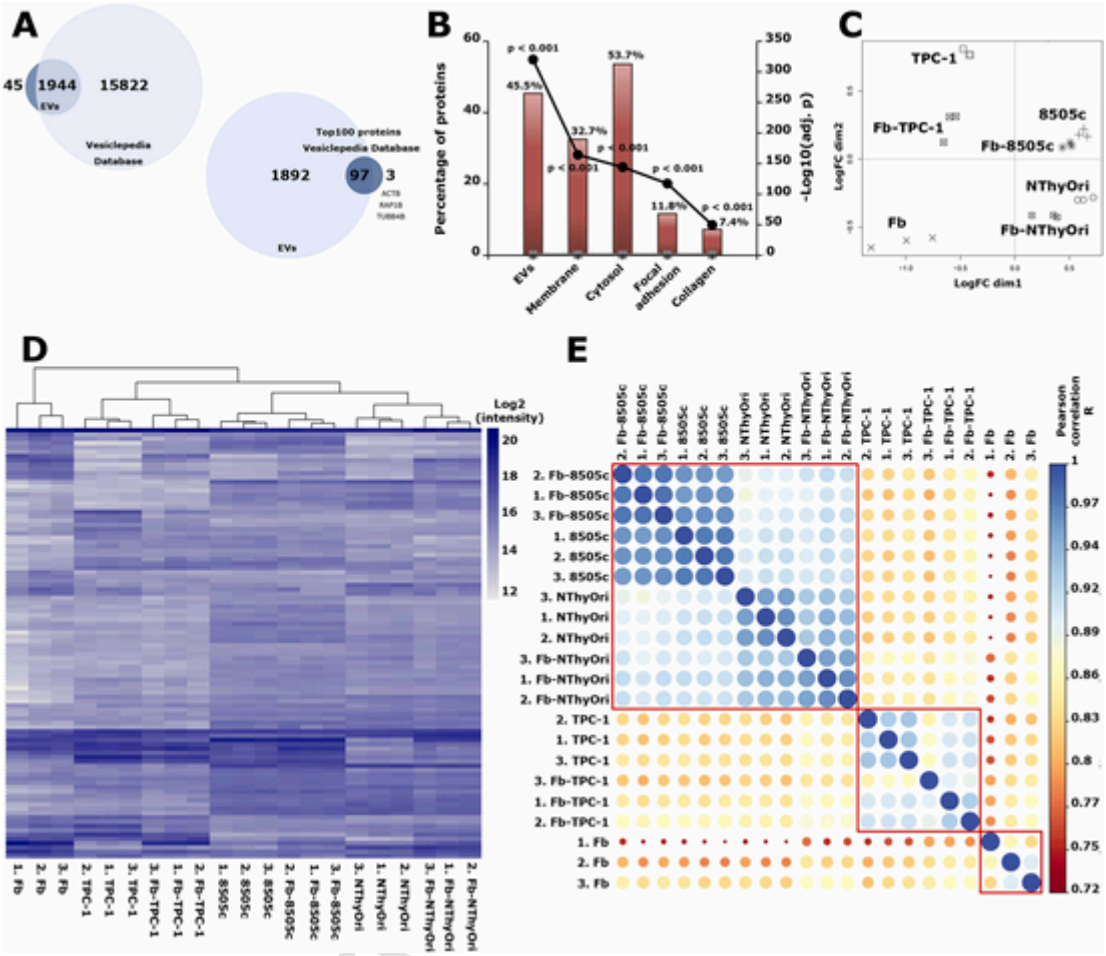

Fig. 2. Proteomic characterization of EVs isolated from Fb, thyroid cells and Fb-thyroid cell co-cultures. (A) Venn diagrams showing the overlap between proteins identified in isolated and co-cultured cell-derived EVs, with all those previously reported and the top 100 most frequent proteins in the Vesiclepedia database. (B) GO-cellular component enrichment analysis of EV-proteome with $p < 0.001$ Benjamini-Hochberg multiple testing FDR correction performed with FunRich and using Uniprot human genome as the background. (C) PCoA of the top 100 identified proteins in the EV-proteome, showing methodological repeatability and the segregation among different samples. (D) Unsupervised hierarchical clustering of the $\log_2$ intensity value of the top 100 identified proteins. (E) Pearson correlation of the all EV-proteome among isolated and co-cultured cells; larger and darker circles depict a higher correlation between samples. PCoA analysis, unsupervised hierarchical clustering, and Pearson correlation performed using R software, showing a robust segregation between EVs from TPC-1/Fb-TPC-1 and 8505c/Fb-8505c, NThyOri/Fb-NThyOri; and the discrimination between EVs from isolated thyroid cells and from Fb-thyroid cell co-cultures.

NThyOri co-cultured cells (Fig. 4C). To note, MMP2 was a shared DEP in the three EV-datasets (Fig. 4A), however, no detectable MMP2 activity was observed in EVs under zymography experimental conditions as was previously described (Bravo-Miana et al., 2020).

3.5. EV trafficking between tumor cells and Fb is more efficient than in non-thyroid tumor environments

In order to study the uptake of EVs, DiI-labeled Fb (Fb^{DiI}) or DiO-labeled TPC-1, 8505c or NThyOri cells ($TPC\text{-}1^{DiO}$, $8505c^{DiO}$, and $NThyOri^{DiO}$) were seeded in the upper chamber of TW dishes, and the uptake of released colored-EVs by recipient cells was evaluated by confocal microscopy and flow cytometry. Fig. 5 shows representative images of the characteristic labeling pattern in recipient Fb (Fig. 5A) and TPC-1 (Fig. 5B) cells after their TW CI co-culture with Fb^{DiI}, $TPC\text{-}1^{DiO}$, and Fb^{DiI}-$TPC\text{-}1^{DiO}$ cells. The dotted pattern, observed in all cultures, is compatible with the uptake of EVs by recipient cells (Lazaro-Ibanez et al., 2017). Moreover, a similar labeling pattern was obtained when $8505c^{DiO}$, Fb^{DiI}-$8505c^{DiO}$, $NThyOri^{DiO}$, and Fb^{DiI}-$NThyOri^{DiO}$ were used as stimuli (data not shown). With the aim of exploring whether the labeled EVs were on the surface or inside the recipient cells, Fb or TPC-1 recipient cells were stained with CD81 to delineate the cell contour, and images were acquired by confocal microscopy. Fig. 5C shows a representative image of Fb co-cultured with $TPC\text{-}1^{DiO}$, where spots-DiO+ (top view, xy) were observed inside the cytoplasm (orthogonal view, xz) of the recipient Fb. A similar pattern, suggestive of intracellular localization of EVs, was observed in recipient TPC-1 cells after their CI co-culture with Fb^{DiI} (Fig. 5D). These results confirm trafficking of EVs between Fb and thyroid cells in culture.

Differences in the potential functionality between EVs from tumoral and non-tumoral contexts have been suggested. To determine whether EVs from thyroid tumoral contexts could also be differentially internalized, recipient Fb and TPC-1 cells were CI co-cultured with Fb^{DiI}, $TPC\text{-}1^{DiO}$, $8505c^{DiO}$, $NThyOri^{DiO}$ and Fb^{DiI}-$TPC\text{-}1^{DiO}$, Fb^{DiI}-$8505c^{DiO}$ and Fb^{DiI}-$NThyOri^{DiO}$ cells, and the percentage of DiI+ or DiO+ recipient cells was evaluated by FACS. In this regard, no differences were detected in the frequency of Fb or TPC-1 DiI+ cells after their CI co-culture with isolated Fb^{DiI} or Fb^{DiI} co-cultured with tumor and non-tumor cells (Fig. S3A and B). Next, we evaluated the frequency of DiO+ recipient cells. Given that no differences were registered between the percentage of Fb DiO+ after their CI co-culture with $TPC\text{-}1^{DiO}$ or Fb^{DiI}-$TPC\text{-}1^{DiO}$ (Fig. S3C1), with $8505c^{DiO}$ or Fb^{DiI}-$8505c^{DiO}$ (Fig. S3C2), or with $NThyOri^{DiO}$ or Fb^{DiI}-$NThyOri^{DiO}$ cells (Fig. S3C3), these results were combined and displayed as TPC-1-tumoral context, 8505c-tumoral context and NThy-

Table 1
Number of DEPs in EVs obtained by the DEqMS method.

DEPs (adj. p < 0.001 and FC ≥ 2)			
EVs from isolated thyroid cells			
Comparison TPC-1 & NThyOri (Table S1)		**Comparison 8505c & NThyOri (Table S3)**	
A. DEPs in EVs from TPC-1	B. DEPs in EVs from NThyOri	A. DEPs in EVs from 8505c	B. DEPs in EVs from NThyOri
97	105	48	20
EVs from Fb-thyroid cells co-culture			
Comparison Fb-TPC-1 & Fb-NThyOri (Table S2)		**Comparison Fb-8505c & Fb-NThyOri (Table S4)**	
A. DEPs in EVs from Fb-TPC-1	B. DEPs in EVs from Fb-NThyOri	A. DEPs in EVs from Fb-8505c	B. DEPs in EVs from Fb-NThyOri
61	49	51	18
DEPs (adj. p < 0.01 and FC ≥ 2) (Table S5)			
EVs from Fb-thyroid cells co-culture vs. EVs from isolated thyroid cells			
Comparison Fb-TPC-1 & TPC-1	**Comparison Fb-8505c & 8505c**		**Comparison Fb-NThyOri & NThyOri**
DEPs in EVs from Fb-TPC-1	DEPs in EVs from Fb-8505c		DEPs in EVs from Fb-NThyOri
25	5		23

DEPs were obtained using the DEqMS method with Benjamini-Hochberg multiple testing FDR correction, using Bioconductor packages in R software, with adj. p < 0.001 or adj. p < 0.01 and FC ≥ 2 between different selected comparisons. FC: fold change. Tables S1-S5: Supplementary Tables 1-5.

Ori-non-tumoral context (Fig. 5E, F). A significant higher frequency of Fb DiO+ was observed after CI co-culture with TPC-1-tumoral compared to NThyOri-non-tumoral contexts (5.2 ± 0.7 vs. 1.5 ± 0.3, respectively, p < 0.05; Fig. 5E). A similar trend was obtained after Fb incubation with isolated- or co-cultured 8505c cells, although no significant differences were found (4.45 ± 0.9 vs. 1.5 ± 0.3, respectively; Fig. 5E). Regarding the TPC-1 DiO+ cells, no changes were detected after their CI co-culture with TPC-1^{DiO+} or NThyOri^{DiO+} isolated or co-cultured with Fb (Fig. 5F and Fig. S3D1 and D2). These findings suggest that in a thyroid tumoral milieu, Fb could uptake a higher quantity of EVs, providing more efficient crosstalk between Fb and thyroid tumor cells.

3.6. Active MMP2 is produced in Fb and TPC-1 CI co-cultures

In tumors, cellular interplay occurs through direct cell-to-cell contact, or indirectly, through paracrine signals and EVs. Therefore, and considering the eventual role of EVs in cell-to-cell communication, MMP2 expression was checked using a CI co-culture strategy. To this end, MMP2 activity was measured in the TW-CMs obtained from isolated Fb and TPC-1 cells, as well as from CI co-cultures of Fb and TPC-1 cells. ProMMP2 and MMP2 activities were detected, with a significant increase in the MMP2/proMMP2 ratio being registered in TW-CMs obtained from (Fb)-(TPC-1) CI co-cultures, respect to Fb and TPC-1 controls (Fig. 6B, C and D).

Previous data have demonstrated that Fb and TPC-1 cells are important for MMP2 expression in the TPC-1 background. Using String database and Cytoscape we found 16 proteins, present in the EV-proteomic data, that exhibited a significant PPI score (1×10^{-16}) with MMP2, denoted as MMP2 interactors in Fig. 6E. Unsupervised hierarchical clustering and the Pearson correlation matrix of MMP2 interactors enabled us to discriminate between EVs derived from thyroid tumor cells and Fb-thyroid tumor cells (TPC-1/8505c and Fb-TPC-1/Fb-8505c) from EVs from non-tumor cells (Fb, NThyOri, Fb-NThyOri). Moreover, this analysis discriminated between Fb-thyroid tumor cell co-culture-derived EVs and isolated thyroid tumor cell-derived EVs (Fig. 6F).

4. Discussion

The importance of fibroblast-tumor cell bidirectional crosstalk, as well as EV release and function, has been shown in different tumor environments (Sahai et al., 2020; Shoucair et al., 2020). In the present work, we characterized for the first time the proteome of EVs from Fb, TPC-1, 8505c and NThyOri cells, as well as their co-cultures with Fb, and described the role of this cellular interplay in EV-cargo and functionality. The results revealed that Fb-thyroid tumor cell crosstalk produces EVs with a biologically relevant-cancer proteome profile, which are specialized in ECM degradation. In contrast, Fb interplay with non-tumor thyroid cells might not provide a stroma remodeling functionality to the secreted EVs, preserving their original message related to cellular metabolism. Supporting this, EVs from thyroid tumoral environments stimulated the synthesis and activation of MMP2 in TME, which could facilitate ECM degradation potentially related to thyroid tumor progression.

Several studies have shown that tumor cells release a higher amount of EVs than their non-tumor counterparts (De Luca et al., 2017; Konig et al., 2017; Osti et al., 2019). In this line, Rappa and co-workers detected a significantly higher number of plasma-EVs from thyroid cancer patients than from healthy controls (Rappa et al., 2019). In contrast, in our cellular model, no differences were detected between the number of EVs derived from TPC-1 and 8505c thyroid tumor cells compared to NThyOri non-tumor cells, in agreement with other reported results (Clos-Garcia et al., 2018; Peinado et al., 2012). However, a significantly higher number of EVs was released from Fb-TPC-1 co-cultures in comparison with EVs obtained from isolated Fb and TPC-1 cells. Regarding these findings, EVs released by tumor cells may be influenced by inner-cell signals or by microenvironmental signals (Bebelman et al., 2018).

In the TME, CAFs represent one of the main stromal components involved in tumor biology, providing all the hallmarks of cancer (Sahai et al., 2020). In this sense, Fb's capacity to promote tumor progression and aggressiveness has been demonstrated in several tumor types, including breast (Chen et al., 2021), lung (Lee et al., 2021) and liver cancers (Affo et al., 2021). Furthermore, in thyroid cancer, CAFs were found to be greatly increased compared with Fb in normal thyroid tissue (Fozzatti and Cheng, 2020). Recently, LOX expression (Boufraqech et al., 2019), COL1A1 deposition, and the concurrent presence of CAFs in association with more aggressive clinicopathological features, have also been described in human thyroid cancer samples (Minna et al., 2020). Despite these findings, evidence that relates Fb-thyroid cell crosstalk to EV secretion is scarce, with studies reporting EVs from thyroid cancer being focused on miRNA cargo (Wang et al., 2020) and with few investigations having considered other biomolecules (Luo et al., 2018). The present findings revealed a characteristic proteomic profile in EVs from Fb-thyroid tumor cell co-cultures, with EV-DEP convergence to the remodeling and homeostasis of the ECM, including ECM organization and structure, ECM interactions, and ECM degradation. Specifically, DEPs in the Fb-TPC-1 background vs. TPC-1 cells were associated with ECM structural constituents and degradation. These interesting functional enrichments suggest that Fb and the bidirectional crosstalk with TPC-1 cells could provide a functional advantage to EVs from the thyroid tumoral milieu, which become specialized in direct communication with the ECM. In this sense, a new paradigm concerning the activity of EVs in the TME contemplates the existence of active crosstalk between EVs and the ECM (Lewin et al., 2020). Consequently, EVs could be considered constitutive elements of ECM, carrying ECM components as well as the enzymes involved in matrix network reorganization. Furthermore, a functional role of ECM-anchored EVs, as a reservoir of intercellular signals that may be released upon matrix remodeling by bystander cells, has also been proposed (Rilla et al., 2019). Moreover, in a comprehensive study, Soekmadji and coworkers (Soekmadji et al., 2020) highlighted the contribution of the interstitial fluid and ECM to tissue derived EVs, that also harbor cell type-specific information, contributing to outline the physiological and/or pathological conditions of an organ.

In turn, an exclusively enriched protein in EVs from Fb-TPC-1 vs. TPC-1 background is MAMDC2. The human protein atlas database describes a positive association between MAMDC2 and thyroid aggres-

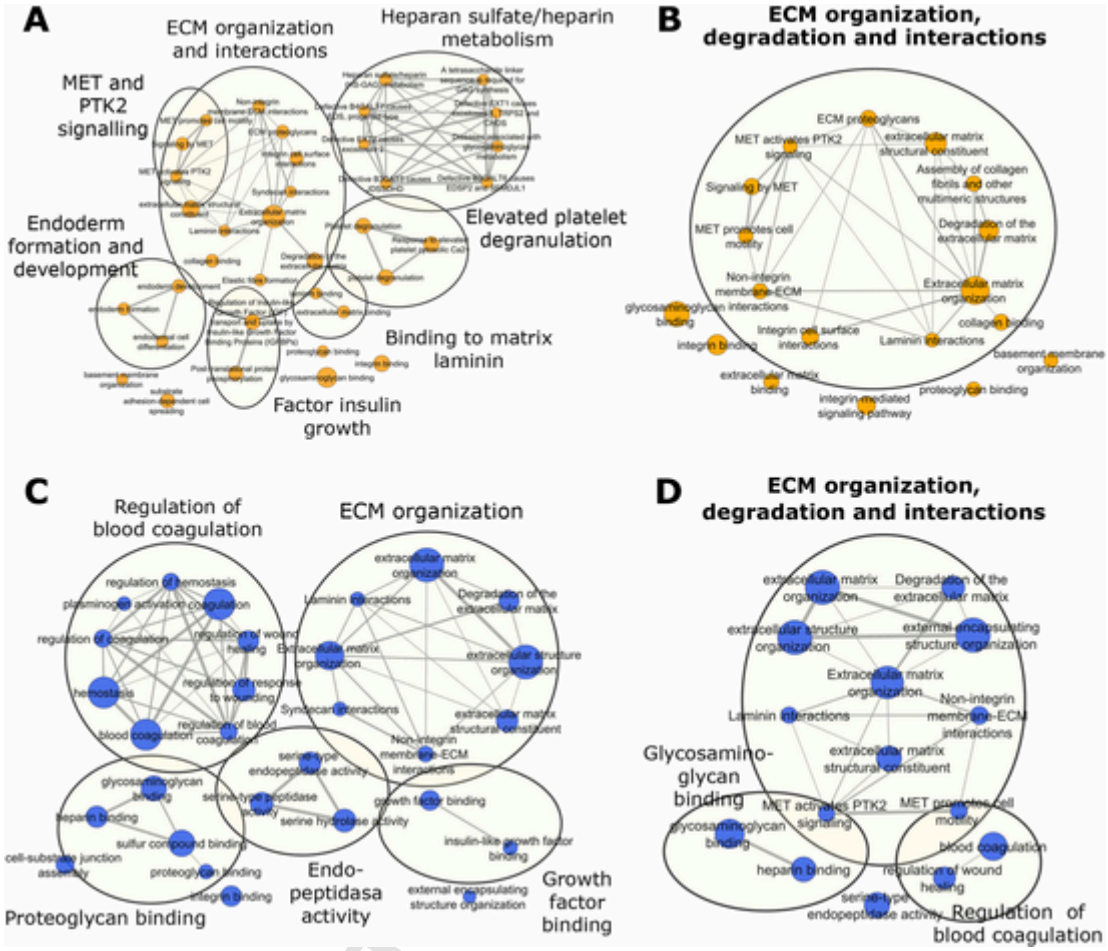

Fig. 3. Fb-TPC-1-and Fb-8505c-derived EVs present a functional convergence in ECM remodeling. ORA analysis of the biological process, molecular function (Gene Ontology terms) and Reactome pathways associated with the DEPs, with adj. $p < 0.001$ and FC ≥ 2 in EVs between samples. Data returned by g:profiler was visualized and interpreted using EnrichmentMap plug-in v3.3.1, ClusterMaker2 and AutoAnnotate v1.3.3 with Markov clustering (MCL cluster) run on Cytoscape v3.8.2. (A) DEPs in EVs from TPC-1 vs. NThyOri, showing their convergence in several clusters. (B) DEPs in EVs from Fb-TPC-1 vs. Fb-NThyOri, showing their convergence in one cluster, associated with ECM remodeling. (C) DEPs in EVs from 8505c vs. NThyOri showing ECM organization and binding enriched terms and (D) Fb-8505c vs Fb-NThyOri, converged in terms related to ECM remodeling. Larger nodes indicate higher number of associated DEPs. MET: protein tyrosine kinase c-Met or hepatocyte growth factor receptor (HGFR). PTK2: protein tyrosine kinase 2 or focal adhesion kinase (FAK).

siveness, making this protein an unfavorable prognostic marker in thyroid cancer. However, further studies would help to shed light on these issues.

The biochemical and proteomic characterization of the EVs revealed an enrichment in CD63 expression in EVs and within DEPs from Fb-TPC-1- and Fb-8505c-tumoral contexts. CD63 participates in the biosynthesis of certain subpopulations of EVs and helps in vesicle identification. Although its functional role is still being debated, it has been shown that tetraspanins participate in directing EV-composition with a specific role in EV-formation, release and internalization by recipient cells (Andreu and Yanez-Mo, 2014; Mathieu et al., 2021). Furthermore, tetraspanins have been associated with tumor progression and metastasis through facilitating and coordinating the function of adhesion receptors and enzymes at the plasma membrane in tumor cells to form tetraspanin-enriched microdomains, thereby promoting multiple cancer stages (Hemler, 2014; Schaper and van Spriel, 2018).

In the present work, evidence has been provided of higher amounts of EVs from thyroid tumor producing cells being taken up by Fb. This finding, although preliminary, suggests that the different EV-uptake by Fb could be related to the EV-quality or their specific cargo. In agreement with our results, Lee and coworkers (Lee et al., 2016) demonstrated that stromal cells, in particular Fb, take up larger numbers of cancer cell-derived EVs compared to epithelial normal cells, with this trafficking being a key regulator of Fb transdifferentiation into an activated form. Accordingly, previous data from our group demonstrated changes in the Fb-phenotype due to Fb-thyroid tumor cell crosstalk (Bravo-Miana et al., 2020; Fozzatti et al., 2019).

In cancerous tissues, ECM provides a niche for tumor cells to live. This ECM network should be properly modified, and to this end, proteinases, such as MMPs, acquire relevance and are carried by EVs or induced and activated in the TME (Rilla et al., 2019). In thyroid cancer, MMPs, specially MMP2 and MMP9, were described as critical effectors of invasion in vitro (Yeh et al., 2006). On the other hand, in PTC patients, the increased expression of MMP2 and MMP9 in tumor tissues was positively correlated with lymph node metastasis (Huang et al., 2017). In addition, other study described serum MMP2 levels as being a predictor of lymph node metastasis and disease persistence/recurrence in PTC patients (Shi et al., 2018). Recently, we demonstrated that cell-to-cell contact in Fb-TPC-1 co-cultures induced MMP2 expression and activity in CMs, and that EVs derived from that environment induced MMP2 expression and activity in Fb (Bravo-Miana et al., 2020). In the present work, MMP2 activity could also be induced in Fb-TPC-1 co-cultures independently of the cell-to-cell contact, which reinforces the role of EVs. Interestingly, the search for MMP2 interactors in the EV-proteome revealed 16 proteins which can discriminate between thyroid microenvironments, and also distinguish Fb-tumor cell interplay in the tumoral milieu. In addition, EVs derived from Fb-TPC-1 co-cultures were able to induce MMP2 expression in non-tumor thyroid cells, con-

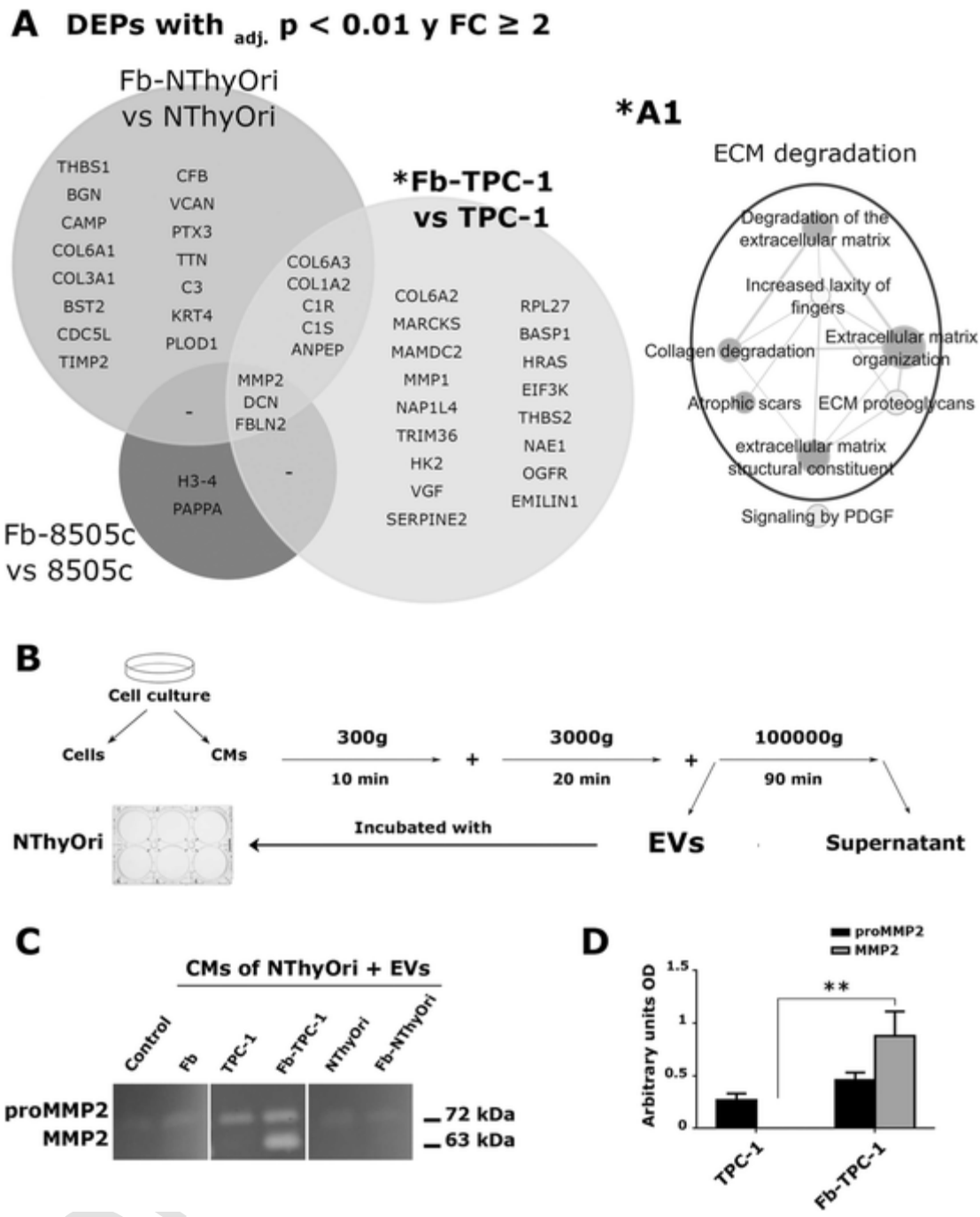

Fig. 4. Fb-TPC-1-derived EVs stimulate MMP2 activity in CMs from NThyOri. (A) Venn diagrams showing DEPs, with adj. $p < 0.01$ and FC ≥ 2, in Fb-TPC-1- vs. TPC-1-, Fb-8505c- vs. 8505c-, and Fb-NThyOri- vs. NThyOri-derived EVs. (*A1) Analysis by ORA and representation by Cytoscape of 25 DEPs in Fb-TPC-1, showing ECM degradation convergence. (B) Schematic representation of EV-preparation and NThyOri + EVs CMs preparation. (C) Representative zymogram showing proMMP2 and MMP2 gelatinolytic activity in NThyOri-CM upon stimulation with medium (control) or EVs (CMs of NThyOri + EVs) from isolated Fb, TPC-1, NThyOri and Fb-TPC-1 and Fb-NThyOri co-cultured cells. Areas of protease activity are indicated by clear bands in the gel for proMMP2 (72 kDa) and MMP2 (63 kDa). (D) Densitometric analysis of proMMP2 and MMP2 in NThyOri-CMs. Results are expressed as the mean of three independent determinations. A significant increase was observed in MMP2 activity in NThyOri-CMs upon stimulation with EVs from Fb-TPC-1 cells vs. EVs from TPC-1 cells (**$p < 0.01$; Kruskal-Wallis test, Dunn's post test). CMs: conditioned media. EVs: extracellular vesicles. CMs of NThyOri + EVs: conditioned media from NThyOri upon stimulation with EVs. OD: optical density.

tributing to the MMP activity in the tumor milieu. In line with this finding, Hardin and coworkers (Hardin et al., 2018) demonstrated that EVs from thyroid cancer stem cells transform NThyOri cells, increasing their proliferation and invasive ability, and inducing epithelial-mesenchymal transition. In agreement with these results, clear modifications in the secretome of tumor-adjacent normal thyroid tissue compared to the tissue-secretome of healthy patients have been described (Robinson et al., 2019).

5. Conclusions

Fb and thyroid tumor cell crosstalk produces specialized EVs with an ECM remodeling proteomic profile, enabling activation of MMP2

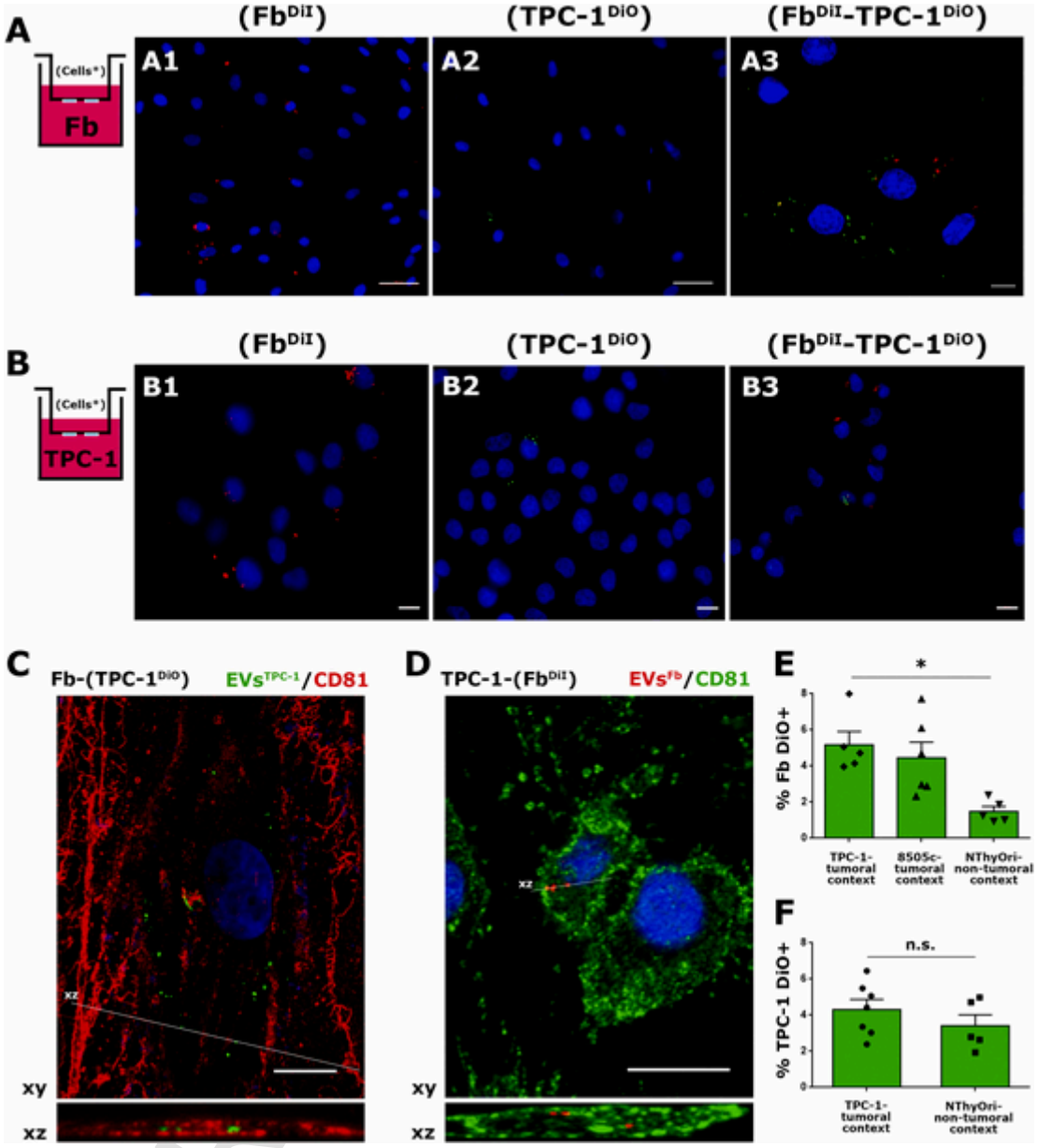

Fig. 5. Fb incorporate a higher number of EVs from tumoral thyroid context than non-tumoral thyroid context. Schematic representation of (A) Fb and (B) TPC-1 recipient cells incubated with Fb^{DiI}, TPC-1^{DiO}, and Fb^{DiI}-TPC-1^{DiO} cells. Representative immunofluorescence images of EV-uptake by Fb incubated with (A1) Fb^{DiI}, (A2) TPC-1^{DiO} and (A3) Fb^{DiI}-TPC-1^{DiO}, and by TPC-1 incubated with (B1) Fb^{DiI}, (B2) TPC-1^{DiO} and (B3) Fb^{DiI}-TPC-1^{DiO}. Isolated or co-cultured-labeled cells in the upper chambers are represented between parentheses (*). The dotted pattern observed in Fb (A1, A2, A3) and TPC-1 (B1, B2, B3) recipient cells is compatible with EV-uptake. Representative confocal images of (C) Fb (after their CI co-culture with TPC-1^{DiO}) and (D) TPC-1 (after their CI co-culture with Fb^{DiI}) recipient cells, after cell-staining with CD81 antibody. Top view (xy) and orthogonal view (xz). Nuclei were stained with DAPI (blue). The orthogonal view (xz) allows visualization of the DiI + signal inside Fb and TPC-1 recipient cells. The quantification of the EV uptake was performed by FACS and expressed as the percentage of (E) Fb DiO + (green) and (F) TPC-1 DiO + (green) recipient cells. A significant increase in the percentage of Fb DiO + was observed after their CI co-culture with TPC-1^{DiO} or Fb^{DiI}-TPC-1^{DiO} (TPC-1-tumoral context), respect to Fb incubated with NThyOri^{DiO} or Fb^{DiI}-NThyOri^{DiO} (NThyOri-non-tumoral context) EV-secreting cells (*$p < 0.05$; Kruskal-Wallis test, Dunn's post test). No differences (n.s.) in EV-uptake were registered in TPC-1 recipient cells. Data are expressed as the mean ± SEM of three independent determinations. n.s.: no significant. Scale bars, 50 μm and 10 μm (A); 10 μm (B); 12 μm (C); 10 μm (D).

and possibly facilitating ECM degradation. The present results provide a background that could be used by future studies aimed at exploring and deciphering how Fb could modify the EV-performance, specifically in the thyroid cancer environment. The knowledge of the bioactive cargo present in EVs, and a better the understanding of their biological function on the TME, could contribute to promoting novel treatment strategies, offering opportunities for minimally invasive diagnostic procedures and the identification of better biomarkers for the diagnosis and the monitoring of the evolution of cancer patients.

Funding

This work was supported by the Secretaría de Ciencia y Tecnología de la Universidad Nacional de Córdoba, Argentina (SECyT-UNC; grant 33620180100476CB; **ACD**); Consejo Nacional de Investigaciones Científicas y Técnicas, Argentina (CONICET; grant 11220150100810CO; **CGP, MMM, ACD**); Fundación Sales, Argentina (**CGP**); and the project RTI2018-094969-B-I00 (MCIU/AEI/FEDER,UE; **JMF-P**). Institutional funding from CONICET, Argentina (Res. 1691/16) is kindly acknowledged.

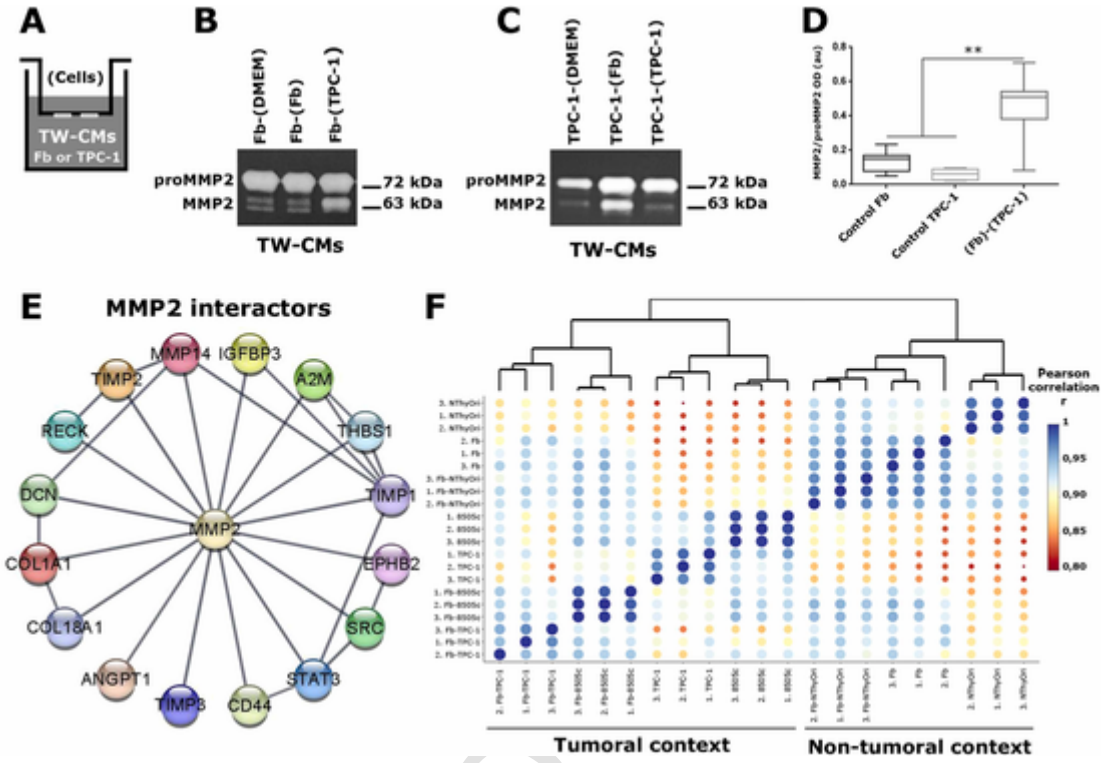

Fig. 6. MMP2 activity in Fb and TPC-1 CI co-cultures and tumoral/non-tumoral stratification with MMP2 interactors. (A) Schematic representation of CI co-cultures of the TW system. Representative zymogram showing proMMP2 and MMP2 gelatinolytic activity in TW-CMs from (B) Fb incubated with (Fb) and (TPC-1); and (C) TPC-1 incubated with (Fb) and (TPC-1) cells. Cells between parentheses represent upper-chamber seeded cells. Areas of protease activity are indicated by clear bands in the gel for proMMP2 (72 kDa) and MMP2 (63 kDa). For comparisons, Fb-(DMEM) and Fb-(Fb) were pooled as Control Fb; TPC-1-(DMEM) and TPC-1-(TPC-1) were pooled as Control TPC-1; Fb-(TPC-1) and TPC-1-(Fb) were pooled as (Fb)-(TPC-1). (D) Densitometric analysis of proMMP2 and MMP2 in TW-CMs from Fb and TPC-1 control and (Fb)-(TPC-1) contact-independent co-culture. Results are expressed as MMP2/proMMP2 mean rate ± SEM of at least four independent determinations. A significant increase in the MMP2/proMMP2 ratio was observed in TW-CMs from (Fb)-(TPC-1) CI co-cultures respect to Fb and TPC-1 controls (**$p < 0.01$; one-way ANOVA, Tukey's post test). (E) MMP2 and MMP2 interactors in the proteome of EVs obtained using String database and Cytoscape v.3.8.2 software. (F) Unsupervised hierarchical clustering of the Pearson correlation values of the MMP2 interactors in EVs derived from isolated and co-cultured cells. MMP2 interactors allow EVs from tumoral and non-tumoral contexts to be discriminated. TW: transwell. OD: optical density. au: arbitrary units.

Data availability

The EV-proteomic dataset generated and supporting the conclusions of this article were deposited in the ProteomeXchange Consortium via the PRIDE partner repository (https://www.ebi.ac.uk/pride) with the dataset identifier PXD028081 ([Dataset] Project DOI: 10.6019/PXD028081). Home-made Script for proteomic analysis is available as a.zip file in Supplementary information and it can be fully run in RStudio v1.4.1717 and R v4.1.2.

Author information

RDCB-M is a research fellow of CONICET and had an international traveling fellowship from IUBMB. MFS was a research fellow of CONICET. DMN-B was a research fellow of FONCYT-Agencia, and at present a research fellow of CONICET. DGC, MMM, CGP and ACD are all staff researchers at CONICET.

Dataset, 2020.

Competing interests

The authors declare that they have no competing interests.

Data availability

The EV-proteomic dataset generated were deposited in the ProteomeXchange Consortium via the PRIDE partner repository with the dataset identifier PXD028081 (Project DOI: 10.6019/PXD028081).

Acknowledgements

The authors thank Dr. Carlos Mas (CEMINCO-CONICET) for his assistance in confocal analysis, Dra. Esperanza Gonzalez (CICbioGUNE, Exosomas Laboratory) and Alejandra Romero, Dra. Laura Gatica, Gabriela Furlán (CIBICI-CONICET) and Estela Salde (IFEC-CONICET) for their excellent technical assistance.

Appendix A. Supporting information

Supplementary data associated with this article can be found in the online version at doi:10.1016/j.ejcb.2022.151254.

References

[Dataset] Proteomics analysis of extracellular vesicles from thyroid tumours, 2020. Project DOI:10.6019/PXD028081.

Uniprot/Swissprot database (UniProt Consortium 2002–2022), n.d. Version 2020_04, 20375 entries.

Affo, S., Nair, A., Brundu, F., Ravichandra, A., Bhattacharjee, S., Matsuda, M., Chin, L., Filliol, A., Wen, W., Song, X., Decker, A., Worley, J., Caviglia, J.M., Yu, L., Yin, D., Saito, Y., Savage, T., Wells, R.G., Mack, M., Zender, L., Arpaia, N., Remotti, H.E., Rabadan, R., Sims, P., Leblond, A.L., Weber, A., Riener, M.O., Stockwell, B.R., Gaublomme, J., Llovet, J.M., Kalluri, R., Michalopoulos, G.K., Seki, E., Sia, D., Chen, X., Califano, A., Schwabe, R.F., 2021. Promotion of cholangiocarcinoma growth by diverse cancer-associated fibroblast subpopulations. e811. Cancer Cell 39, 866–882. https://doi.org/10.1016/j.ccell.2021.03.012.

Andreu, Z., Yanez-Mo, M., 2014. Tetraspanins in extracellular vesicle formation and function. Front. Immunol. 5, 442. https://doi.org/10.3389/fimmu.2014.00442.

Bebelman, M.P., Smit, M.J., Pegtel, D.M., Baglio, S.R., 2018. Biogenesis and function of extracellular vesicles in cancer. Pharmacol. Ther. 188, 1–11. https://doi.org/10.1016/j.pharmthera.2018.02.013.

Bertero, T., Oldham, W.M., Grasset, E.M., Bourget, I., Boulter, E., Pisano, S., Hofman, P., Bellvert, F., Meneguzzi, G., Bulavin, D.V., Estrach, S., Feral, C.C., Chan, S.Y., Bozec, A., Gaggioli, C., 2019. Tumor-stroma mechanics coordinate amino acid availability to sustain tumor growth and malignancy. e110. Cell Metab. 29, 124–140. https://doi.org/10.1016/j.cmet.2018.09.012.

Boufraqech, M., Patel, D., Nilubol, N., Powers, A., King, T., Shell, J., Lack, J., Zhang, L., Gara, S.K., Gunda, V., Klubo-Gwiezdzinska, J., Kumar, S., Fagin, J., Knauf, J., Parangi, S., Venzon, D., Quezado, M., Kebebew, E., 2019. Lysyl oxidase is a key player in BRAF/MAPK pathway-driven thyroid cancer aggressiveness. Thyroid Off. J. Am. Thyroid. Assoc. 29, 79–92. https://doi.org/10.1089/thy.2018.0424.

Bravo-Miana, R.D.C., Della Vedova, A.B., De Paul, A.L., Remedi, M.M., Guantay, M.L., Gilardoni, M.B., Pellizas, C.G., Donadio, A.C., 2020. Thyroid tumor cells-fibroblasts crosstalk: role of extracellular vesicles. Endocr. Connect. 9, 506–518. https://doi.org/10.1530/EC-20-0113.

Chen, B., Sang, Y., Song, X., Zhang, D., Wang, L., Zhao, W., Liang, Y., Zhang, N., Yang, Q., 2021. Exosomal miR-500a-5p derived from cancer-associated fibroblasts promotes breast cancer cell proliferation and metastasis through targeting USP28. Theranostics 11, 3932–3947. https://doi.org/10.7150/thno.53412.

Clos-Garcia, M., Loizaga-Iriarte, A., Zuniga-Garcia, P., Sanchez-Mosquera, P., Rosa Cortazar, A., Gonzalez, E., Torrano, V., Alonso, C., Perez-Cormenzana, M., Ugalde-Olano, A., Lacasa-Viscasillas, I., Castro, A., Royo, F., Unda, M., Carracedo, A., Falcon-Perez, J.M., 2018. Metabolic alterations in urine extracellular vesicles are associated to prostate cancer pathogenesis and progression. J. Extracell. Vesicles 7, 1470442. https://doi.org/10.1080/20013078.2018.1470442.

De Luca, L., D'Arena, G., Simeon, V., Trino, S., Laurenzana, I., Caivano, A., La Rocca, F., Villani, O., Mansueto, G., Deaglio, S., Innocenti, I., Laurenti, L., Molica, S., Pietrantuono, G., De Stradis, A., Del Vecchio, L., Musto, P., 2017. Characterization and prognostic relevance of circulating microvesicles in chronic lymphocytic leukemia. Leuk. Lymphoma 58, 1424–1432. https://doi.org/10.1080/10428194.2016.1243790.

Fozzatti, L., Cheng, S.Y., 2020. Tumor cells and cancer-associated fibroblasts: a synergistic crosstalk to promote thyroid cancer. Endocrinol. Metab. 35, 673–680. https://doi.org/10.3803/EnM.2020.401.

Fozzatti, L., Alamino, V.A., Park, S., Giusiano, L., Volpini, X., Zhao, L., Stempin, C.C., Donadio, A.C., Cheng, S.Y., Pellizas, C.G., 2019. Interplay of fibroblasts with anaplastic tumor cells promotes follicular thyroid cancer progression. Sci. Rep. 9, 8028. https://doi.org/10.1038/s41598-019-44361-6.

Hardin, H., Helein, H., Meyer, K., Robertson, S., Zhang, R., Zhong, W., Lloyd, R.V., 2018. Thyroid cancer stem-like cell exosomes: regulation of EMT via transfer of lncRNAs. Lab. Investig. J. Tech. Methods Pathol. 98, 1133–1142. https://doi.org/10.1038/s41374-018-0065-0.

Hemler, M.E., 2014. Tetraspanin proteins promote multiple cancer stages. Nat. Rev. Cancer 14, 49–60. https://doi.org/10.1038/nrc3640.

Huang, L.L., Wang, Z., Cao, C.J., Ke, Z.F., Wang, F., Wang, R., Luo, C.Q., Lu, X., Wang, L.T., 2017. AEG-1 associates with metastasis in papillary thyroid cancer through upregulation of MMP2/9. Int. J. Oncol. 51, 812–822. https://doi.org/10.3892/ijo.2017.4074.

Jeppesen, D.K., Fenix, A.M., Franklin, J.L., Higginbotham, J.N., Zhang, Q., Zimmerman, L.J., Liebler, D.C., Ping, J., Liu, Q., Evans, R., Fissell, W.H., Patton, J.G., Rome, L.H., Burnette, D.T., Coffey, R.J., 2019. Reassessment of exosome composition. e418. Cell 177, 428–445. https://doi.org/10.1016/j.cell.2019.02.029.

Jolly, L.A., Novitskiy, S., Owens, P., Massoll, N., Cheng, N., Fang, W., Moses, H.L., Franco, A.T., 2016. Fibroblast-mediated collagen remodeling within the tumor microenvironment facilitates progression of thyroid cancers driven by BrafV600E and Pten loss. Cancer Res. 76, 1804–1813. https://doi.org/10.1158/0008-5472.CAN-15-2351.

Kitahara, C.M., Sosa, J.A., 2020. Understanding the ever-changing incidence of thyroid cancer. Nat. Rev. Endocrinol. 16, 617–618. https://doi.org/10.1038/s41574-020-00414-9.

Konig, L., Kasimir-Bauer, S., Bittner, A.K., Hoffmann, O., Wagner, B., Santos Manvailer, L.F., Kimmig, R., Horn, P.A., Rebmann, V., 2017. Elevated levels of extracellular vesicles are associated with therapy failure and disease progression in breast cancer patients undergoing neoadjuvant chemotherapy. Oncoimmunology 7, e1376153. https://doi.org/10.1080/2162402X.2017.1376153.

Kowal, J., Arras, G., Colombo, M., Jouve, M., Morath, J.P., Primdal-Bengtson, B., Dingli, F., Loew, D., Tkach, M., Thery, C., 2016. Proteomic comparison defines novel markers to characterize heterogeneous populations of extracellular vesicle subtypes. Proc. Natl. Acad. Sci. USA 113, E968–E977. https://doi.org/10.1073/pnas.1521230113.

Lazaro-Ibanez, E., Neuvonen, M., Takatalo, M., Thanigai Arasu, U., Capasso, C., Cerullo, V., Rhim, J.S., Rilla, K., Yliperttula, M., Siljander, P.R., 2017. Metastatic state of parent cells influences the uptake and functionality of prostate cancer cell-derived extracellular vesicles. J. Extracell. Vesicles 6, 1354645. https://doi.org/10.1080/20013078.2017.1354645.

Lee, S., Hong, J.H., Kim, J.S., Yoon, J.S., Chun, S.H., Hong, S.A., Kim, E.J., Kang, K., Lee Kang, J., Ko, Y.H., Ahn, Y.H., 2021. Cancer-associated fibroblasts activated by miR-196a promote the migration and invasion of lung cancer cells. Cancer Lett. 508, 92–103. https://doi.org/10.1016/j.canlet.2021.03.021.

Lee, T.H., Chennakrishnaiah, S., Meehan, B., Montermini, L., Garnier, D., D'Asti, E., Hou, W., Magnus, N., Gayden, T., Jabado, N., Eppert, K., Majewska, L., Rak, J., 2016. Barriers to horizontal cell transformation by extracellular vesicles containing oncogenic H-ras. Oncotarget 7, 51991–52002. https://doi.org/10.18632/oncotarget.10627.

Lewin, S., Hunt, S., Lambert, D.W., 2020. Extracellular vesicles and the extracellular matrix: a new paradigm or old news. Biochem. Soc. Trans. 48, 2335–2345. https://doi.org/10.1042/BST20200717.

Luo, D., Zhan, S., Xia, W., Huang, L., Ge, W., Wang, T., 2018. Proteomics study of serum exosomes from papillary thyroid cancer patients. Endocr. Relat. Cancer 25, 879–891. https://doi.org/10.1530/ERC-17-0547.

Maman, S., Witz, I.P., 2018. A history of exploring cancer in context. Nat. Rev. Cancer 18, 359–376. https://doi.org/10.1038/s41568-018-0006-7.

Mathieu, M., Nevo, N., Jouve, M., Valenzuela, J.I., Maurin, M., Verweij, F.J., Palmulli, R., Lankar, D., Dingli, F., Loew, D., Rubinstein, E., Boncompain, G., Perez, F., Thery, C., 2021. Specificities of exosome versus small ectosome secretion revealed by live intracellular tracking of CD63 and CD9. Nat. Commun. 12, 4389. https://doi.org/10.1038/s41467-021-24384-2.

Minna, E., Brich, S., Todoerti, K., Pilotti, S., Collini, P., Bonaldi, E., Romeo, P., Cecco, L., Dugo, M., Perrone, F., Busico, A., Vingiani, A., Bersani, I., Anichini, A., Mortarini, R., Neri, A., Pruneri, G., Greco, A., Borrello, M.G., 2020. Cancer associated fibroblasts and senescent thyroid cells in the invasive front of thyroid carcinoma. Cancers 12. https://doi.org/10.3390/cancers12010112.

Osti, D., Del Bene, M., Rappa, G., Santos, M., Matafora, V., Richichi, C., Faletti, S., Beznoussenko, G.V., Mironov, A., Bachi, A., Fornasari, L., Bongetta, D., Gaetani, P., DiMeco, F., Lorico, A., Pelicci, G., 2019. Clinical significance of extracellular vesicles in plasma from glioblastoma patients. Clin. Cancer Res. Off. J. Am. Assoc. Cancer Res. 25, 266–276. https://doi.org/10.1158/1078-0432.CCR-18-1941.

Pathan, M., Keerthikumar, S., Chisanga, D., Alessandro, R., Ang, C.S., Askenase, P., Batagov, A.O., Benito-Martin, A., Camussi, G., Clayton, A., Collino, F., Di Vizio, D., Falcon-Perez, J.M., Fonseca, P., Fonseka, P., Fontana, S., Gho, Y.S., Hendrix, A., Hoen, E.N., Iraci, N., Kastaniegaard, K., Kislinger, T., Kowal, J., Kurochkin, I.V., Leonardi, T., Liang, Y., Llorente, A., Lunavat, T.R., Maji, S., Monteleone, F., Overbye, A., Panaretakis, T., Patel, T., Peinado, H., Pluchino, S., Principe, S., Ronquist, G., Royo, F., Sahoo, S., Spinelli, C., Stensballe, A., Thery, C., van Herwijnen, M.J.C., Wauben, M., Welton, J.L., Zhao, K., Mathivanan, S., 2017. A novel community driven software for functional enrichment analysis of extracellular vesicles data. J. Extracell. Vesicles 6, 1321455. https://doi.org/10.1080/20013078.2017.1321455.

Pathan, M., Fonseka, P., Chitti, S.V., Kang, T., Sanwlani, R., Van Deun, J., Hendrix, A., Mathivanan, S., 2019. Vesiclepedia 2019: a compendium of RNA, proteins, lipids and metabolites in extracellular vesicles. Nucleic Acids Res. 47, D516–D519. https://doi.org/10.1093/nar/gky1029.

Peinado, H., Aleckovic, M., Lavotshkin, S., Matei, I., Costa-Silva, B., Moreno-Bueno, G., Hergueta-Redondo, M., Williams, C., Garcia-Santos, G., Ghajar, C., Nitadori-Hoshino, A., Hoffman, C., Badal, K., Garcia, B.A., Callahan, M.K., Yuan, J., Martins, V.R., Skog, J., Kaplan, R.N., Brady, M.S., Wolchok, J.D., Chapman, P.B., Kang, Y., Bromberg, J., Lyden, D., 2012. Melanoma exosomes educate bone marrow progenitor cells toward a pro-metastatic phenotype through MET. Nat. Med. 18, 883–891. https://doi.org/10.1038/nm.2753.

Petersen, T.N., Brunak, S., von Heijne, G., Nielsen, H., 2011. SignalP 4.0: discriminating signal peptides from transmembrane regions. Nat. Methods 8, 785–786. https://doi.org/10.1038/nmeth.1701.

Quintero-Fabian, S., Arreola, R., Becerril-Villanueva, E., Torres-Romero, J.C., Arana-Argaez, V., Lara-Riegos, J., Ramirez-Camacho, M.A., Alvarez-Sanchez, M.E., 2019. Role of matrix metalloproteinases in angiogenesis and cancer. Front. Oncol. 9, 1370. https://doi.org/10.3389/fonc.2019.01370.

Rappa, G., Puglisi, C., Santos, M.F., Forte, S., Memeo, L., Lorico, A., 2019. Extracellular vesicles from thyroid carcinoma: the new frontier of liquid biopsy. Int. J. Mol. Sci. 20. https://doi.org/10.3390/ijms20051114.

Reimand, J., Isserlin, R., Voisin, V., Kucera, M., Tannus-Lopes, C., Rostamianfar, A., Wadi, L., Meyer, M., Wong, J., Xu, C., Merico, D., Bader, G.D., 2019. Pathway enrichment analysis and visualization of omics data using g:Profiler, GSEA, Cytoscape and EnrichmentMap. Nat. Protoc. 14, 482–517. https://doi.org/10.1038/s41596-018-0103-9.

Rilla, K., Mustonen, A.M., Arasu, U.T., Harkonen, K., Matilainen, J., Nieminen, P., 2019. Extracellular vesicles are integral and functional components of the extracellular matrix. Matrix Biol. J. Int. Soc. Matrix Biol. 75–76, 201–219. https://doi.org/10.1016/j.matbio.2017.10.003.

Robinson, J.L., Feizi, A., Uhlen, M., Nielsen, J., 2019. A systematic investigation of the malignant functions and diagnostic potential of the cancer secretome. e2625. Cell Rep. 26, 2622–2635. https://doi.org/10.1016/j.celrep.2019.02.025.

Royo, F., Moreno, L., Mleczko, J., Palomo, L., Gonzalez, E., Cabrera, D., Cogolludo, A., Vizcaino, F.P., van-Liempd, S., Falcon-Perez, J.M., 2017. Hepatocyte-secreted extracellular vesicles modify blood metabolome and endothelial function by an arginase-dependent mechanism. Sci. Rep. 7, 42798. https://doi.org/10.1038/srep42798.

Sahai, E., Astsaturov, I., Cukierman, E., DeNardo, D.G., Egeblad, M., Evans, R.M., Fearon, D., Greten, F.R., Hingorani, S.R., Hunter, T., Hynes, R.O., Jain, R.K., Janowitz, T., Jorgensen, C., Kimmelman, A.C., Kolonin, M.G., Maki, R.G., Powers, R.S., Pure, E., Ramirez, D.C., Scherz-Shouval, R., Sherman, M.H., Stewart, S., Tlsty, T.D., Tuveson, D.A., Watt, F.M., Weaver, V., Weeraratna, A.T., Werb, Z., 2020. A framework for advancing our understanding of cancer-associated fibroblasts. Nat. Rev. Cancer 20, 174–186. https://doi.org/10.1038/s41568-019-0238-1.

Saitoh, O., Mitsutake, N., Nakayama, T., Nagayama, Y., 2009. Fibroblast-mediated in vivo and in vitro growth promotion of tumorigenic rat thyroid carcinoma cells but not normal Fisher rat thyroid follicular cells. Thyroid Off. J. Am. Thyroid. Assoc. 19, 735–742. https://doi.org/10.1089/thy.2009.0017.

Schaper, F., van Spriel, A.B., 2018. Antitumor immunity is controlled by tetraspanin proteins. Front. Immunol. 9, 1185. https://doi.org/10.3389/fimmu.2018.01185.

Shi, Y., Su, C., Hu, H., Yan, H., Li, W., Chen, G., Xu, D., Du, X., Zhang, P., 2018. Serum MMP-2 as a potential predictive marker for papillary thyroid carcinoma. PLoS One 13, e0198896. https://doi.org/10.1371/journal.pone.0198896.

Shoucair, I., Weber Mello, F., Jabalee, J., Maleki, S., Garnis, C., 2020. The role of cancer-associated fibroblasts and extracellular vesicles in tumorigenesis. Int. J. Mol. Sci. 21. https://doi.org/10.3390/ijms21186837.

Siegel, R.L., Miller, K.D., Fuchs, H.E., Jemal, A., 2021. Cancer statistics, 2021. CA Cancer J. Clin. 71, 7–33. https://doi.org/10.3322/caac.21654.

Soekmadji, C., Li, B., Huang, Y., Wang, H., An, T., Liu, C., Pan, W., Chen, J., Cheung, L., Falcon-Perez, J.M., Gho, Y.S., Holthofer, H.B., Le, M.T.N., Marcilla, A., O'Driscoll, L., Shekari, F., Shen, T.L., Torrecilhas, A.C., Yan, X., Yang, F., Yin, H., Xiao, Y., Zhao, Z., Zou, X., Wang, Q., Zheng, L., 2020. The future of Extracellular Vesicles as Theranostics - an ISEV meeting report. J. Extracell. Vesicles 9, 1809766. https://doi.org/10.1080/20013078.2020.1809766.

Szklarczyk, D., Gable, A.L., Lyon, D., Junge, A., Wyder, S., Huerta-Cepas, J., Simonovic, M., Doncheva, N.T., Morris, J.H., Bork, P., Jensen, L.J., Mering, C.V., 2019. STRING v11: protein-protein association networks with increased coverage, supporting functional discovery in genome-wide experimental datasets. Nucleic Acids Res. 47, D607–D613. https://doi.org/10.1093/nar/gky1131.

Tkach, M., Kowal, J., Thery, C., 2018. Why the need and how to approach the functional diversity of extracellular vesicles. Philos. Trans. R. Soc. Lond. Ser. B Biol. Sci. 373. https://doi.org/10.1098/rstb.2016.0479.

Tyanova, S., Temu, T., Sinitcyn, P., Carlson, A., Hein, M.Y., Geiger, T., Mann, M., Cox, J., 2016. The Perseus computational platform for comprehensive analysis of (prote) omics data. Nat. Methods 13, 731–740. https://doi.org/10.1038/nmeth.3901.

van Niel, G., D'Angelo, G., Raposo, G., 2018. Shedding light on the cell biology of extracellular vesicles. Nat. Rev. Mol. Cell Biol. 19, 213–228. https://doi.org/10.1038/nrm.2017.125.

Wang, Y., Xu, F., Zhong, J.Y., Lin, X., Shan, S.K., Guo, B., Zheng, M.H., Yuan, L.Q., 2020. Exosomes as mediators of cell-to-cell communication in thyroid disease. Int. J. Endocrinol. 2020, 4378345. https://doi.org/10.1155/2020/4378345.

Winkler, J., Abisoye-Ogunniyan, A., Metcalf, K.J., Werb, Z., 2020. Concepts of extracellular matrix remodelling in tumour progression and metastasis. Nat. Commun. 11, 5120. https://doi.org/10.1038/s41467-020-18794-x.

Wisniewski, J.R., Zougman, A., Mann, M., 2009. Combination of FASP and StageTip-based fractionation allows in-depth analysis of the hippocampal membrane proteome. J. Proteome Res. 8, 5674–5678. https://doi.org/10.1021/pr900748n.

Yeh, M.W., Rougier, J.P., Park, J.W., Duh, Q.Y., Wong, M., Werb, Z., Clark, O.H., 2006. Differentiated thyroid cancer cell invasion is regulated through epidermal growth factor receptor-dependent activation of matrix metalloproteinase (MMP)-2/gelatinase A. Endocr. Relat. Cancer 13, 1173–1183. https://doi.org/10.1677/erc.1.01226.

Zhu, Y., Orre, L.M., Zhou Tran, Y., Mermelekas, G., Johansson, H.J., Malyutina, A., Anders, S., Lehtio, J., 2020. DEqMS: a method for accurate variance estimation in differential protein expression analysis. Mol. Cell. Proteom. MCP 19, 1047–1057. https://doi.org/10.1074/mcp.TIR119.001646.